NUCL SCI TECH (2019) 30:105
https://doi.org/10.1007/s41365-019-0628-9

Power losses caused by longitudinal HOMs in 1.3-GHz cryomodule of SHINE

Jun-Jie Guo[1,2] · Qiang Gu[1,3] · Meng Zhang[3] · Zhen Wang[3] · Jian-Hao Tan[1,3]

Received: 1 January 2019 / Revised: 22 March 2019 / Accepted: 31 March 2019 / Published online: 4 June 2019

Abstract Shanghai high-repetition-rate XFEL and extreme light facility (SHINE), the first hard XFEL based on a superconducting accelerated structure in China, is now under development at the Shanghai Institute of Applied Physics, Chinese Academy of Sciences. In this paper, power losses caused by trapped longitudinal high-order modes (HOM), steady-state loss, and transient loss generated by untrapped HOMs in the 1.3-GHz SHINE cryomodule are investigated and calculated. The heat load generated by resistive wall wakefields is considered as well. Results are presented for power losses of every element in the 1.3-GHz cryomodule, caused by HOM excitation in the acceleration RF system of the continuous-wave linac of SHINE.

Keywords Power loss · Higher-order modes (HOMs) · Resistive wall wakefields · Impedance · Superconducting cavities

This work was supported by the Frontier Research of Large Science Installation (2016YFA0401902) and the Youth Innovation Promotion Association CAS (No. 2018300).

✉ Jun-Jie Guo
guojunjie@sinap.ac.cn

Qiang Gu
guqiang@sinap.ac.cn

[1] Shanghai Institute of Applied Physics, Chinese Academy of Sciences, Shanghai 201800, China

[2] University of Chinese Academy of Sciences, Beijing 100049, China

[3] Shanghai Advanced Research Institute, Chinese Academy of Sciences, Shanghai 201210, China

1 Introduction

Currently, the first hard XFEL in China is under construction in Shanghai. This is called the Shanghai high-repetition-rate XFEL and extreme light facility (SHINE) [1–3], which is a superconducting accelerated structure-based FEL device. In the future, SHINE will provide hard coherent X-ray radiation for a broad spectrum of basic research applications [4]. Superconducting RF (SRF) technology has been chosen in order to minimize the power consumption and operational cost of the facility because SHINE is required to operate in the continuous-wave (CW) regime.

While the use of superconducting accelerating cavities in large particle accelerator facilities offers many advantages in areas such as RF efficiency and feasible beam parameter ranges, a major expense of operating such a machine is the power required of the cryogenic plant. Consideration must be given to minimizing both the static and dynamic heat loads. One element of the latter, particularly relevant in a high-current, short-bunch CW facility, is higher-order-mode (HOM) electromagnetic field power generated by the beam when passing through the cavities and beamline elements. Therefore, the power losses generated by HOMs owing to monopole HOMs are the subject of calculations.

The paper is organized as follows. In Sect. 2, the machine layout and main parameters of the SHINE linac and the geometry of the 1.3-GHz cryomodule in SHINE are introduced briefly. In Sect. 3, power losses caused by trapped HOMs in the Tesla cavity of the 1.3-GHz SHINE cryomodule are investigated. In Sect. 4, the distribution of the heat load caused by untrapped HOMs and the resistive wake in every element of the 1.3-GHz SHINE cryomodule

are calculated. The steady-state loss and transient loss [5] caused by untrapped HOMs in the 1.3-GHz SHINE cryomodule are investigated as well. Section 5 summarizes the results and significance of this paper.

2 Linac of SHINE

The linac schematic of SHINE is shown in Fig. 1a [6]. The main accelerating elements of the SHINE linac are Tesla 1.3-GHz nine-cell elliptical cavities [7]. The linac is segmented into four sections named L0, L1, L2, and L3. The number of elements and their nominal operational RF parameters in each section are summarized in Table 1. An idealized beam current spectrum without time or charge jitter is calculated.

In this section, the 1.3-GHz cryomodule of SHINE is considered. The cryomodule contains beam line interconnections (bellows, gate valves, and a beam line absorber) as shown in Fig. 1b [8] and Fig. 1c [9]. The 1.3-GHz cryomodule of SHINE comprises eight nine-cell cavities each with an active length of 1.036 m, 3.5-cm iris radius, and 3.9-cm beam tube radius. Between the cavities are bellows that are roughly 5.5 cm long and have nine convolutions.

3 Trapped longitudinal HOM

An electromagnetic field will be excited by the bunch behind it when an electron bunch passes through the cavity. This electromagnetic field is called a wakefield in the time domain and a high-order mode in the frequency domain and can be divided into longitudinal and transverse HOMs according to the component on the coordinate axis. Power losses of every element in a 1.3-GHz cryomodule are mainly caused by longitudinal HOMs, which is the main research object of this paper. A longitudinal HOM can be characterized as a trapped or untrapped HOM by its relation to the beam pipe cutoff frequency. The frequency of a trapped HOM is below f_{cutoff}, while an untrapped HOM has a frequency above f_{cutoff}. This section focuses on trapped HOMs, and untrapped HOMs are considered in the next section.

As we know, a trapped longitudinal HOM below the beam pipe cutoff frequency of Tesla SRF cavities causes heat, adds to the cryogenic losses, and increases the operational cost of a linac, which is excited when the beam traverses the SRF cavity. Interaction of the beam spectrum with the cavity HOM spectrum leads to power losses in the SRF cavity. Thus, the beam spectrum and cavity HOM spectrum are calculated in the next section.

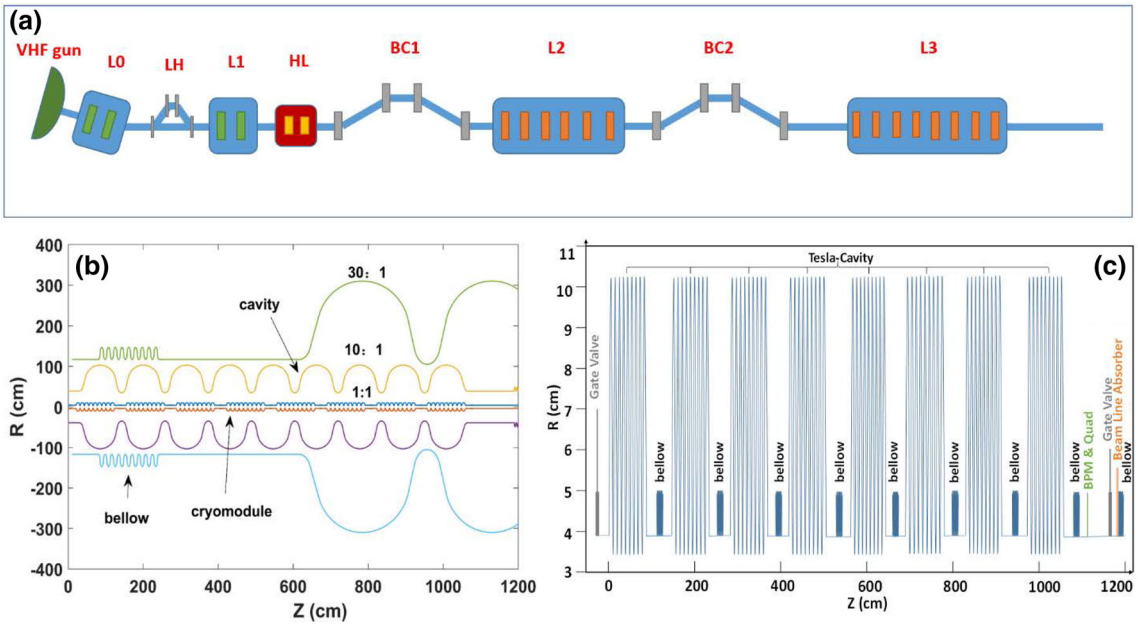

Fig. 1 (Color online) **a** Schematic layout of SHINE main linac and geometry of 1.3-GHz Tesla cavity cryomodule with **b** bellows and **c** interconnections. Tesla superconducting cavity is made of pure niobium, beam line pipe is copper plated, and gate valve and flange of interconnection part are made of stainless steel

Table 1 Configuration of each section in SHINE linac

	No. of cryomodules	Avail. cavities	Powered cavities	Gradient (MV/m)	E_{out} (MeV)	σ_z (Q_b = 100 pC) (mm)	σ_z (Q_b = 300 pC) (mm)
L1	2	16	15	14.8	326	1	3
L2	18	144	135	15.5	2148	0.14	0.42
L3	54	432	406	15.5	8653	0.007	0.021

3.1 Beam spectrum

The amplitude and frequency of the main lines of the beam current spectrum directly affect the probability and intensity of HOMs in SRF accelerating structures.

Two cases of the beam in the SHINE are considered in this paper: Case 1 and Case 2. In Case 1, the bunch repetition frequency is assumed to be constant and equal to 1 MHz and total change Q_b = 300 pC. In Case 2, the bunch repetition frequency is assumed to be constant and equal to 0.6 MHz and total change Q_b = 100 pC. The calculated beam spectra of Case 1 and Case 2 are shown in Fig. 2.

3.2 Cavity HOM spectrum

The spectra and impedance of the higher-order modes in the SHINE are evaluated in this section. The main contribution of HOM loss comes from the frequency mode with the highest impedance and a frequency approaching the main line of the beam spectrum.

The HOM spectrum of a 1.3-GHz Tesla-type cavity is evaluated by using a CST simulation [10]. For longitudinal monopole modes, the cutoff frequency in a cylindrical pipe is defined as $f_{\text{cutoff}} = 2\pi c\frac{X_{01}}{r} \approx 2\pi c\frac{2.4048}{r}$, where X_{01} is the first root of $J_0(r)$, the Bessel function of the first kind of order 0. According to the above formula, the cutoff frequency of a 1.3-GHz Tesla-type cavity is equal to 2.94 GHz. The spectrum and *R/Q* of a 1.3-GHz Tesla-type cavity are shown in Fig. 3a, b, respectively.

3.3 Power loss calculation

The beam traversing a cavity excites various modes of the cavity. The main accelerating mode will be compensated, but there are also high-order modes in the cavity. The excitation of HOMs leads to losses of beam power. In addition, it is necessary to know which modes are used to evaluate these losses. Given the shapes of the cavities, all needed information can be obtained by using a CST

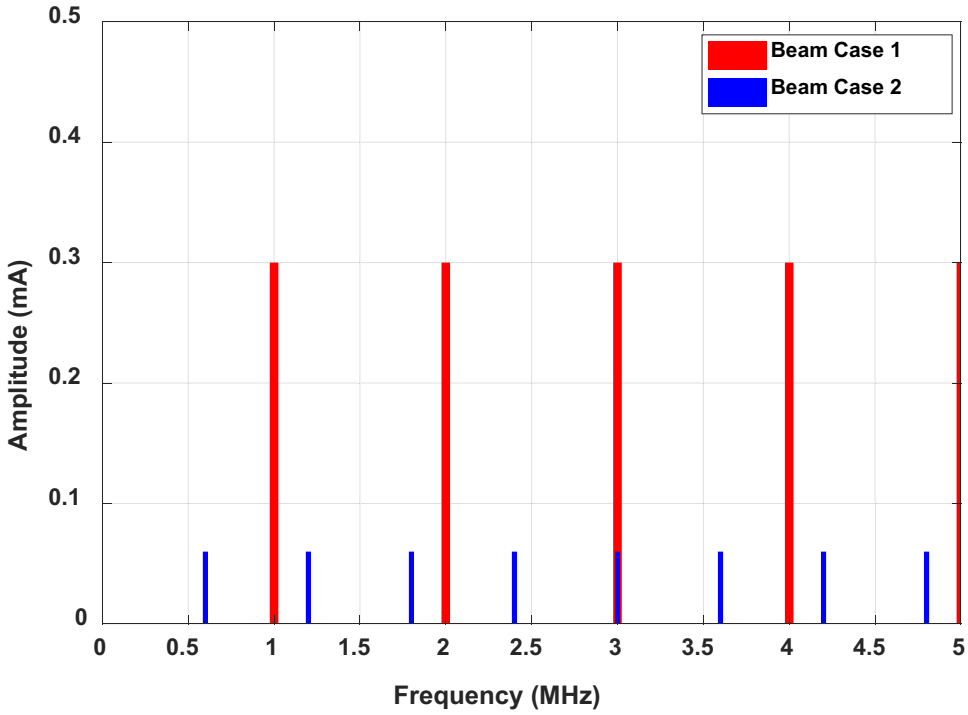

Fig. 2 (Color online) Idealized beam spectrum of Beam Cases 1 and 2

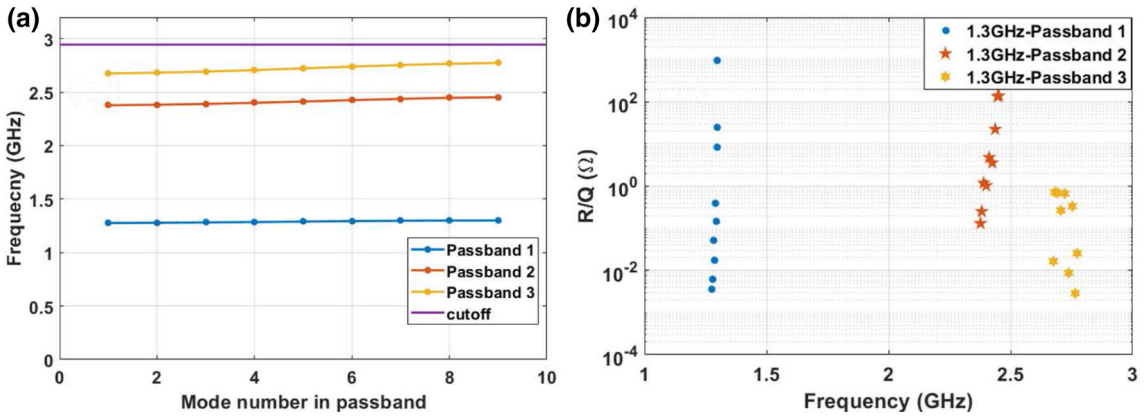

Fig. 3 (Color online) **a** Spectrum and **b** impedance of monopole HOMs in 1.3-GHz Tesla-type cavity

simulation. After that, power losses are calculated as described in the following.

According to Ref. [11], the surface resistance of superconducting Nb is

$$R_{\mathrm{s}} = R_{\mathrm{res}} + R_{\mathrm{BCS}}, \tag{1}$$

where R_{res} = 10 nΩ and the BCS part is parameterized as

$$R_{\mathrm{BCS}}\ (\Omega) = 2 \times 10^{-4} \frac{1}{T\ (\mathrm{K})} \left(\frac{f_n\ (\mathrm{GHz})}{1.5} \right)^2 \mathrm{e}^{\frac{-17.67}{T\ (\mathrm{K})}}. \tag{2}$$

Trapped modes may have a higher value of Q_{h} [12], where Q_{h} is the loaded quality factor of the HOMs. The following Q_{h} values are used in our analysis: $Q_{\mathrm{h}} = 2 \times 10^5$, 1×10^6, and 1×10^7. The HOM frequency spread owing to the manufacturing mechanical tolerances will be considered in our simulation. The total power loss in the cavity walls is calculated as the sum of losses by the individual beam harmonics.

The power losses can be calculated as [13]

$$P = \sum_{n=1}^{N} \sum_{m=1}^{M} \left(\frac{\tilde{I}_n^2}{8W} \right) \left(\frac{R}{Q} \right)_m \frac{R_{\mathrm{s}} \omega_m^3 A_{mm}}{(\omega_n^2 - \omega_m^2)^2 + \left(\frac{\omega_n \omega_m}{Q_{\mathrm{h}}} \right)^2}, \tag{3}$$

where

$$A_{mm} = \oint H_m^2(z)\mathrm{d}s = \int_0^L 2\pi r(\ell) H_m^2(\ell)\mathrm{d}\ell. \tag{4}$$

3.4 Results

To accurately estimate the probability of resonance HOM excitation in a SHINE linear accelerator by the beam component, a statistical analysis must be carried out. This analysis requires the propagation of data for the HOM parameters (frequency, impedance, and quality factor). Thus, the manufacturing mechanical tolerances will be taken into account in order to obtain this information. The acceleration mode should be perfectly adjusted, so a frequency of exactly 1.3 GHz is used in calculations. About 3000 random runs are made for each cavity in order to estimate the probability of the RF losses per cryomodule [14].

The distributions of power loss for the two beam cases in a 1.3-GHz Tesla-type cavity are shown in Fig. 4a, b, respectively.

4 Untrapped longitudinal HOM

As mentioned in the previous section, a longitudinal HOM above the cutoff frequency is called an untrapped longitudinal HOM, which can propagate through the cryomodule. This will cause a heat load in every element of the cryomodule. These elements include the cavity, bellows, beam line absorber (BLA) [15], fundamental power coupler (FPC), high-order mode coupler (HOMC) [16], gate valve, flange, and cryomodule (CM) pipe. In this section, power losses caused by untrapped longitudinal HOMs (including the resistive wall wake [17]) are considered and calculated together.

4.1 HOM power generated in SHINE linac

When an electron bunch traverses the 1.3-GHz cryomodule shown in Fig. 2, its wake energy is radiated into modes (untrapped longitudinal HOMs) that are much higher than the cutoff frequency. The primary source of excitation of untrapped longitudinal HOMs in the SHINE is the irises of nine-cell cavities (called a geometric wake). In addition, another source is generated by resistive wall wakefields in the 1.3-GHz cryomodule beam pipe of the SHINE.

The HOM power generated by the beam is

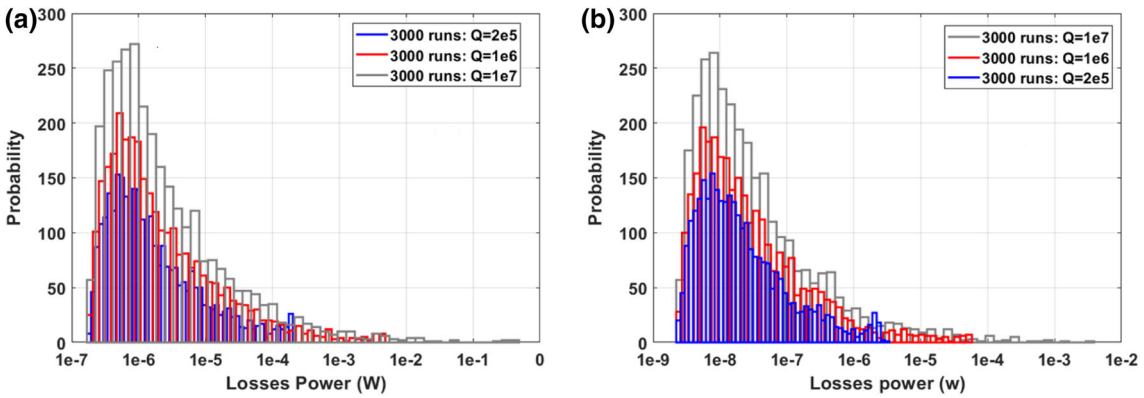

Fig. 4 (Color online) Calculations of power losses in 1.3-GHz Tesla-type cavity for **a** Beam Case 1 and **b** Beam Case 2

$$P = Q^2 f_{\mathrm{rep}} K_{\mathrm{loss}}. \tag{5}$$

In the SHINE, the maximum HOM power is generated for Case Q_{b} = 300 pC and f_{rep} = 1 MHz and the minimum HOM power is generated for Case Q_{b} = 100 pC and f_{rep} = 0.6 MHz. Thus, the above two cases are considered in this section.

According to Eq. (5), we need a K_{loss} parameter, which is defined by the following equation:

$$K_{\mathrm{loss}} = \frac{1}{q}\int_{-\infty}^{+\infty} W_{\parallel}(s)\lambda(s)\mathrm{d}s, \tag{6}$$

where q is the bunch charge, $W_{\parallel}(s)$ is the longitudinal wake potential, and $\lambda(s)$ is the bunch distribution, which usually has a Gaussian distribution [18].

The longitudinal wake potential is a convolution of a longitudinal wake function and bunch distribution is described in the following equation:

$$W_{\parallel}(s) = \frac{1}{q}\int_{-\infty}^{+\infty} w_{\parallel}(s-s')\lambda(s')\mathrm{d}s', \tag{7}$$

where $w_{\parallel}(s)$ is the wake function of a point-like charge.

In a periodic structure, a short-range wake can be approximated by [8, 19]

$$w_{\parallel} = A\frac{Z_0 C}{\pi^2 a}\exp\left(-\sqrt{\frac{s}{s_0}}\right). \tag{8}$$

The 1.3-GHz SHINE linac can be considered a multi-periodic structure: The first elementary period is the cavity cell, the second is the nine-cell cavity with a bellows and beam tubes, and the third is the cryomodule, which houses eight cavities with nine bellows. Thus, Eq. (8) can be used in our calculation.

4.2 Steady-state wake losses

When the beam enters the first cryomodule in a string, it will first encounter transient wakefields that gradually change to steady-state wakes. The change occurs over a distance on the order of the catch-up distance, $Z_{\mathrm{cu}} = a^2/2\sigma_z$. For the SHINE, the catch-up distance Z_{cu} = 0.2, 1.5, and 29 m and Z_{cu} = 0.6, 4.4, and 87.5 m in the L1, L2, and L3 sections for Beam Case 1 and Beam Case 2, respectively. According to Fig. 2, the length of a 1.3-GHz cryomodule is about 12 m. To reach a steady-state solution, 1, 1, and 3 cryomodules need to be considered in the L1, L2, and L3 sections for Beam Case 1. Similarly, 1, 1, and 8 cryomodules need to be considered in the L1, L2, and L3 sections for Beam Case 2. Therefore, the wake function is fitted by calculating the wake potentials of different σ_z bunches in the chain of eight cryomodules with ECHO [20], which is shown in Fig. 5 [21].

From the fit of the numerical data to Eq. (8), we obtain the following equation:

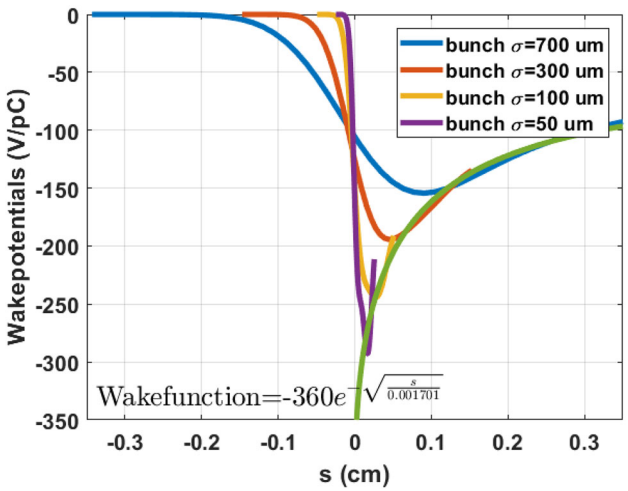

Fig. 5 (Color online) Longitudinal wake potential and fitted wake function in eighth cryomodule

$$w_{\parallel}(s) = 360\exp\left(-\sqrt{\frac{s}{0.001701}}\right). \quad (9)$$

In this section, Beam Case 1 and Beam Case 2 in the L3 part are primarily considered in our calculations. The wake potential is calculated by the convolution of the longitudinal wake function and Gaussian bunch distribution shown in Fig. 6a, b for Beam Case 1 and Beam Case 2, respectively [22].

With the above wake potential, $K_{\rm loss}$ can be calculated according to Eq. (6). For an RMS bunch length of 1 mm, 0.14 mm, and 7 μm in L1, L2, and L3, the loss factor is 89, 137, and 169 V/pC per cryomodule, respectively. The steady-state HOM power generated for $Q_{\rm b}$ = 100 pC and $f_{\rm rep}$ = 0.6 MHz (Beam Case 2) is 0.54, 0.82, and 1.01 W/Cryomodule, respectively.

For an RMS bunch length of 3 mm, 0.42 mm, and 21 μm in L1, L2, and L3 for Beam Case 1, the loss factor is 57, 113, and 162 V/pC per cryomodule, respectively. The steady-state HOM power generated for $Q_{\rm b}$ = 300 pC and $f_{\rm rep}$ = 1 MHz for Beam Case 1 is 5.12, 10.17, and 14.55 W/Cryomodule, respectively.

4.3 Transient wake losses

As mentioned in Sect. 4.2, the beam wake reaches a steady-state wake in sections L1 and L2 as long as the beam traverses one cryomodule owing to the catch-up distance. To reach a steady-state solution, however, a structure of eight cryomodules with a total length of 96 m needs to be considered when the beam traverses the L3 section. Thus, transient wake losses generated by a 7-μm beam in L3 are the focus of our calculations.

When the 7-μm beam enters the first cell of the first cavity of the first cryomodule in L3, the wake induced is well approximated by a diffraction model. In subsequent cells and cavities, the wake gradually reaches its steady state. According to the diffraction model, the loss factor for a Gaussian bunch traversing the first cell of a cavity is given by [5]

$$k_{\rm cell} = 0.723\frac{Z_0 c}{\sqrt{2}\pi^2 a}\sqrt{\frac{g}{\sigma_{\rm z}}}, \quad (10)$$

where g is the cell gap. For a 1.3-GHz cryomodule in L3, a = 35 mm (the cell iris radius), g = 89 mm, and $\sigma_{\rm z}$ = 7 μm. Using Eq. (10), we find that $k_{\rm cell}$ = 18.9 V/pC is the contribution of the first cell. For the first cavity, the diffraction model gives this value multiplied by the number of cells in a cavity: $k_{\rm cavity}$ = 170.1 V/pC.

To estimate the loss factor, k_n, we consider the model [5]

$$k_n = \sum_{m=1}^{8}\bar{k}_{nm} = \frac{1}{9}\sum_{m=1}^{8}\sum_{p=1}^{9}[\bar{k}_{\rm tr}{\rm e}^{-\alpha_{nmp}} + \bar{k}_{\rm ss}(1-{\rm e}^{-\alpha_{nmp}})], \quad (11)$$

where m is the cavity number and p is the cell number. $\bar{k}_{\rm tr}$ and $\bar{k}_{\rm ss}$ are, respectively, the transient and steady-state cavity loss factors, and $\alpha_{nmp} = [72(n-1)+9(m-1)+p-1]/9d_{\rm c}$, where $d_{\rm c}$ is the declination per cavity of the transient component. The transient loss factor $\bar{k}_{\rm tr}$ is given by the diffraction Eq. (10), where $\sigma_{\rm z}$ = 7 μm, and is then multiplied by 9 (the number of cells in a cavity) so that the value of $\bar{k}_{\rm tr}$ is 170.1 V/pC per cavity.

$\bar{k}_{\rm ss}$ is taken from Sect. 4.2. $K_{\rm loss}$ = 169 V/pC per cryomodule. Divided by 8 (the number of cavities in a cryomodule), the value of $\bar{k}_{\rm ss}$ is 21.13 V/pC per cavity. Note that the declination $d_{\rm c}$ is equivalent to a distance of 8.93 m, which is much shorter than the catch-up distance $Z_{\rm cu}$ = 87.5 m, the distance after which the wake experienced by the beam is within a few percent of the steady-state wakes.

Taking $\bar{k}_{\rm tr}$ = 170.1 V/pc (from the diffraction model), $\bar{k}_{\rm ss}$ = 21.13 V/pc (from Sect. 4.2), and $d_{\rm c}$ = 8.93 m, we obtain the result that for the first ten cryomodules, the loss

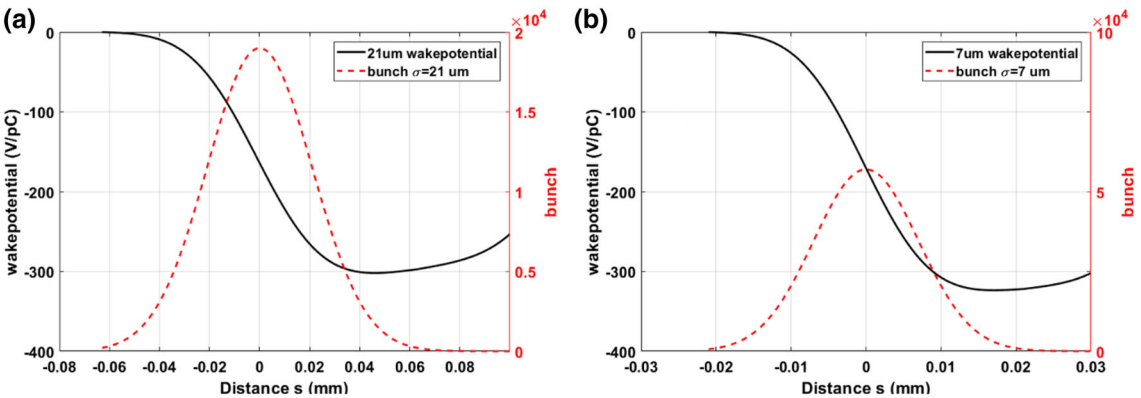

Fig. 6 (Color online) Wake potential and bunch distribution for a bunch length of $\sigma_{\rm z}$ = 21 μm for **a** Beam Case 1 and **b** $\sigma_{\rm z}$ = 7 μm for Beam Case 2 owing to 1.3-GHz cryomodule

factor and power losses by the 100-pC beam at 1 MHz are shown in Fig. 7a and Table 2.

It is known from Fig. 7a and Table 2 that K_{loss} is unchanged from the eighth cryomodule of L3, and K_{loss} is decremented from the first cryomodule to the eighth cryomodule. That is to say, after the beam traverses the eighth cryomodule, it reaches the steady state.

For completeness, the calculations for the beam passing through the initial cryomodules of L1 and L2 in Beam Case 2 are repeated. We find that in L1, the loss in the first cryomodule is 0.54 W, and the result for all the others is 0.54 W. In L2, the loss in the first cryomodule is 0.86 W, and the result for all the others is 0.82 W.

Similarly, the loss factor and power losses in L3 of Beam Case 1 are calculated again in the same way as shown in Fig. 7b and Table 3. For completeness, the calculations for the beam passing through the initial cryomodules of L1 and L2 in Beam Case 1 are repeated. We find that in L1, the loss in the first cryomodule is 5.13 W, and the result for all the others is 5.12 W. In L2, the loss in the first cryomodule is 10.32 W, and the result for all the others is 10.17 W.

4.4 HOM power spectrum

In order to understand the distribution of power among the modes, the HOM power spectrum can be evaluated using the following equation [9]:

$$\frac{\mathrm{d}P}{\mathrm{d}\omega} = Q_{\mathrm{b}}^2 f_{\mathrm{rep}} Z_{\parallel}(\omega) \exp\left(-\left(\frac{\omega\sigma_z}{c}\right)^2\right), \tag{12}$$

where $Z_{\parallel}$ is the longitudinal wake impedance. $Z_{\parallel}$ can be obtained by performing a Fourier transform on the wake function. Figure 8 shows the differential HOM power spectra for Beam Cases 1 and 2 in the 1.3-GHz cryomodule of the SHINE linac.

The frequency range of the excited modes can be approximated as

$$\omega \approx \frac{c}{\sigma_z}. \tag{13}$$

In the SHINE linac, the bunch length is as short as 7 μm, and the spectrum of the HOM frequency extends up to terahertz. In order to estimate the fraction of HOM power dissipating at 2 K in the cryomodule, the total HOM power can be determined as the sum of two parts, i.e.,

$$P_{\mathrm{total}} = \int_0^{\omega_{\mathrm{c}}} \frac{\mathrm{d}P}{\mathrm{d}\omega}\mathrm{d}\omega + \int_{\omega_{\mathrm{c}}}^{\omega} \frac{\mathrm{d}P}{\mathrm{d}\omega}\mathrm{d}\omega, \tag{14}$$

where the first term is the power below the cutoff frequency (ω_{c}). This power is effectively extracted from the operating environment using HOM couplers. The second term in Eq. (14) corresponds to HOMs that have frequencies above the cutoff frequency and is called the untrapped HOM power. According to Eqs. (12) and (14), the untrapped HOM power of Beam Case 1 for L1, L2, and L3 is 3.47, 8.34, and 12.95 W/Cryomodule, respectively. Similarly, the untrapped HOM power of Beam Case 2 for L1, L2, and L3 is 0.43, 0.70, and 0.938 W/Cryomodule, respectively.

4.5 Power loss generated by resistive wall wakefields in cryomodule beam pipe

Another source of beam power loss is the resistive wall wakefields in the 1.3-GHz cryomodule beam pipe of SHINE. Because the beam pipe is maintained at cryogenic temperatures, resistive wall effects are typically weak or, more commonly, they enter the anomalous skin effect regime (ASE) where the AC conductivity of metals is substantially different from the normal skin effect (NSE). The beam pipe of the 1.3-GHz cryomodule in SHINE is round. The impedance in this case is in the form of Ref. [17]:

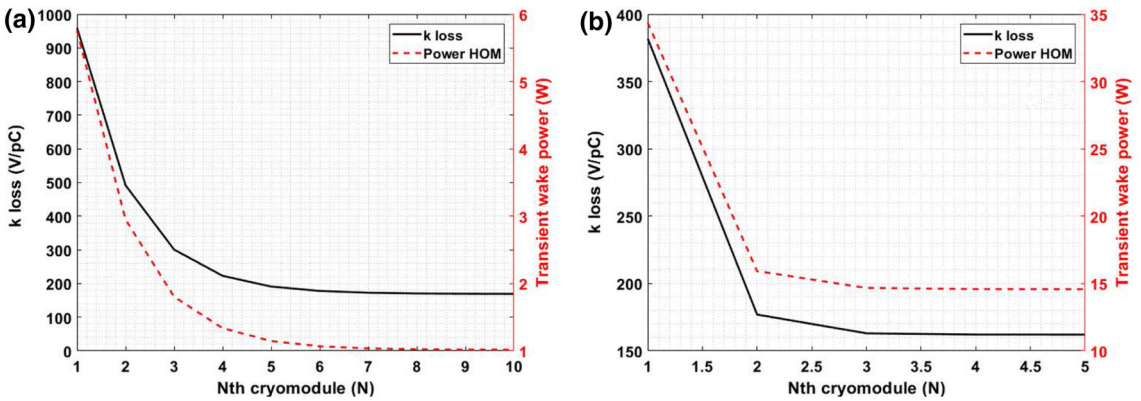

Fig. 7 K_{loss} and transient wake power of nth cryomodule for **a** $\sigma_z = 7$ μm and **b** $\sigma_z = 21$ μm bunches

Table 2 K_{loss} and transient wake power of ten cryomodules for Beam Case 2 in L3

Nth cryomodule	1	2	3	4	5	6	7	8	9	10
K_{loss} (V/pC)	959	491	300	221	190	177	172	169	169	169
P_wake (W)	5.76	2.95	1.80	1.34	1.15	1.068	1.036	1.01	1.01	1.01

Table 3 K_{loss} and transient wake power of five cryomodules for Beam Case 1 in L3

Nth cryomodule	1	2	3	4	5
K_{loss} (V/pC)	382	177	163	162	162
P_wake (W)	34.37	15.92	14.67	14.55	14.55

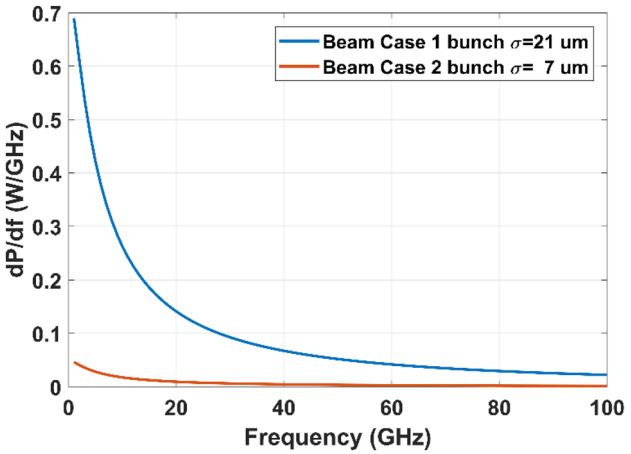

Fig. 8 (Color online) Differential power spectrum about Beam Case 1 (blue) and Beam Case 2 (red) in 1.3-GHz cryomodule of SHINE linac

$$Z_{\parallel}(k) = \frac{Z_0}{2\pi a}\left(\frac{1}{\zeta(k)} - \frac{ika}{2}\right)^{-1}, \tag{15}$$

where a is the inner radius of the beam pipe and $\zeta(k)$ can be known from Ref. [17]. From Eq. (15), we obtain the real and imaginary parts of the impedance as a function of the frequency for copper and for a pipe of radius a = 39 mm, which is shown in Fig. 9. Then, according to Eq. (12), the power density spectra for the resistive wall wakefields in Beam Cases 1 and 2 in the 1.3-GHz cryomodule beam pipe of the SHINE linac are calculated and shown in Fig. 10.

4.6 Diffusion model

One way to estimate the distribution of the HOM power absorption is to use a diffusion-like model [9] in which the radiation fills the available volume like a gas. This is a good approximation that is well above the cutoff frequency and where the surface reflection coefficient is close to unity.

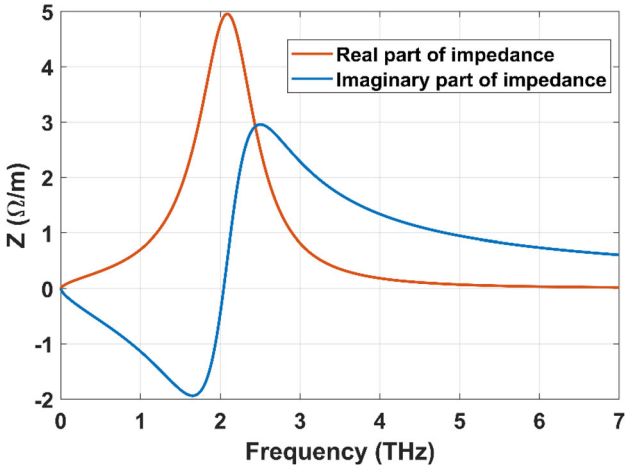

Fig. 9 (Color online) Real (red lines) and imaginary (blue lines) parts of impedance for copper (the residual resistivity ratio (RRR) = 30 [17])

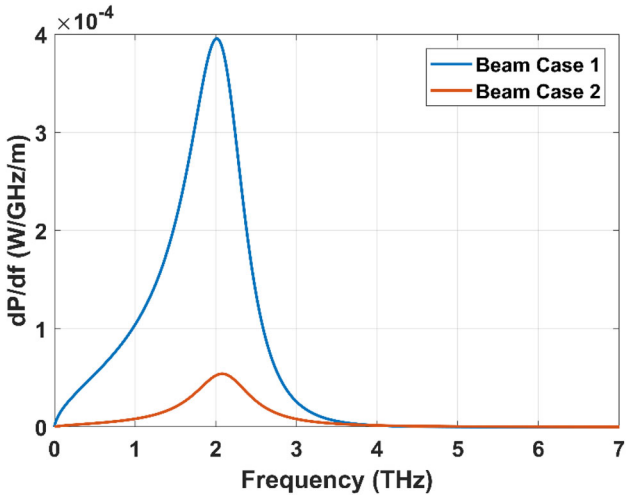

Fig. 10 (Color online) Differential power spectrum about Beam Case 1 (blue) and Beam Case 2 (red) in 1.3-GHz cryomodule beam pipe of SHINE linac

The power absorption is proportional to the impedance of the element:

$$I_i^{\mathrm{abs}}(\omega) \approx n_i S_i \frac{\mathrm{d}P(\omega)}{\mathrm{d}\omega}\mathrm{Re}(Z_i(\omega))\mathrm{d}\omega, \tag{16}$$

where S_i is the surface area of the ith element, i is the type of element (such as a cavity, bellows, or beam pipe), n is the number of elements, ω is the angular frequency, $\frac{\mathrm{d}p(\omega)}{\mathrm{d}\omega}$ is the HOM spectral density, and $\mathrm{Re}(Z_i(\omega))$ is the real part of the surface impedance.

The power absorbed by the ith-type element is

$$P_i = \int_0^\infty \frac{\mathrm{d}P}{\mathrm{d}\omega} \frac{I_i^{\mathrm{abs}}(\omega)}{\sum I_i^{\mathrm{abs}}(\omega)} \mathrm{d}\omega. \tag{17}$$

In the end, we have to count the total power loss that contains the power loss $P_{\mathrm{geom\_wake}}$ of the untrapped longitudinal HOMs generated by the geometric wakefield and the heat load $P_{\mathrm{resis\_wake}}$ of the resistive wake generated by the resistive wall of the beam pipe.

4.7 Surface impedance of elements

The surface impedance of a superconducting Nb cavity can be found in Eq. (1) in Sect. 3.3. The surface impedance of steel is computed using

$$R_{\mathrm{ss}}(\omega) = \mathrm{Re}\left(\frac{1+i}{\sqrt{2}}\sqrt{\frac{\omega\mu_0}{k}}\right), \tag{18}$$

where k is the electrical conductivity. We used $k = 10^6\ \Omega^{-1}\ \mathrm{m}^{-1}$ for stainless steel.

Copper exhibits anomalous effects at 4 K at higher frequencies:

$$R_{\mathrm{cu}}(\omega) = \mathrm{Re}\left(A\omega^{\frac{2}{3}}\left(1+i\sqrt{3}\right)\right), \tag{19}$$

where $A = 3.3 \times 10^{-10}\ \Omega\ \mathrm{s}^{2/3}$.

The surface impedance of the absorber, R_{absorber}, can be calculated in the following way [23]:

$$\begin{aligned} \alpha(\omega) &= \frac{\omega\sqrt{\xi_{\mathrm{r}}'\mu_{\mathrm{r}}'} \times \sqrt{\sqrt{1+\tan(\delta_{\mathrm{d}})^2}-1}}{c\sqrt{2}}, \\ \tan(\delta_{\mathrm{d}}) &= \frac{\xi_{\mathrm{r}}''}{\xi_{\mathrm{r}}'}; \quad \delta_{\mathrm{s}} = \frac{1}{\alpha}, \\ k &= \xi_{\mathrm{r}}''\xi_0\omega; \quad R_{\mathrm{absorb}} = \frac{1}{k\delta_{\mathrm{s}}}, \end{aligned} \tag{20}$$

where α is the attenuation coefficient in a lossy medium; ξ_{r}' and ξ_{r}'' are the real and imaginary parts of the relative electrical permittivity, respectively; and μ_{r}' is the relative permeability. Aluminum nitride ceramic is chosen as the absorber material. The loss tangent for this material is larger than 0.4, and $\xi_{\mathrm{r}}' < 30$.

Calculation formulas for the equivalent impedance of the radiation elements are derived from [24]:

$$\begin{aligned} \mathrm{d}P_n(\omega) &= P_0(1-\exp(-2\alpha_n\ell)), \\ \alpha_n(\omega) &= \frac{Z(\omega)}{Z_0 r\sqrt{1-\left(\frac{\omega C_n}{\omega}\right)^2}}, \\ \mathrm{d}P(\omega) &= \sum_{n=1}^{N(\omega)} \mathrm{d}P_n(\omega). \end{aligned} \tag{21}$$

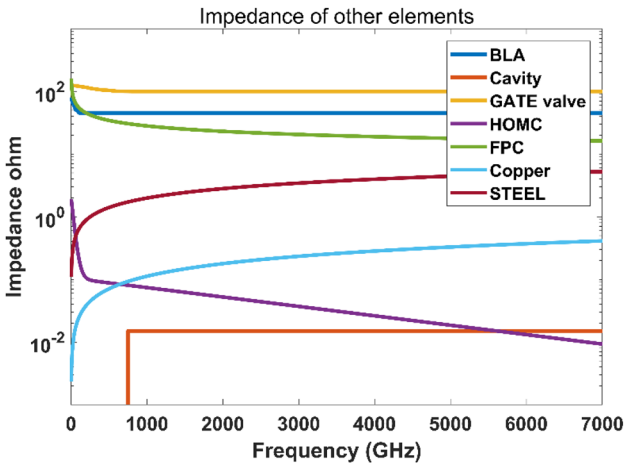

Fig. 11 (Color online) Equivalent surface impedances of beamline components and impedance of cavity and copper and steel materials

The equivalent surface impedances for all of the beam line components can be obtained by solving Eq. (21). The result is shown in Fig. 11 with a comparison of the impedances of the stainless steel, copper, and superconducting cavity.

4.8 Distribution of untrapped radiation in 1.3-GHz cryomodule

Using Eqs. (16) and (17), the dependence of the surface impedance on the frequency and HOM differential power spectrum, and the distribution of the total power loss (including the power loss $P_{\mathrm{geom\_wake}}$ of the untrapped longitudinal HOMs generated by the geometric wakefield and the heat load $P_{\mathrm{resis\_wake}}$ of the resistive wake generated by the resistive wall of the beam pipe), in every element of the 1.3-GHz cryomodule are shown in Fig. 12a, b for Beam Cases 1 and Case 2, respectively.

From Fig. 12, it can be observed that most of the power is deposited to the beam line absorber placed outside the operating temperature of 2 K. Only a small fraction is dissipated at 2 K, and this is distributed among different elements (such as the cavity, flanges, and bellows) when there is no radiation loss to the coupler ports. If the radiation loss is considered, then the power losses are uniformly distributed between the fundamental power coupler (FPC) and the beam line absorber.

5 Conclusion

In the SHINE linac, based on a superconducting accelerated structure, power losses generated by the beam passing through the linac may not be negligible. Therefore,

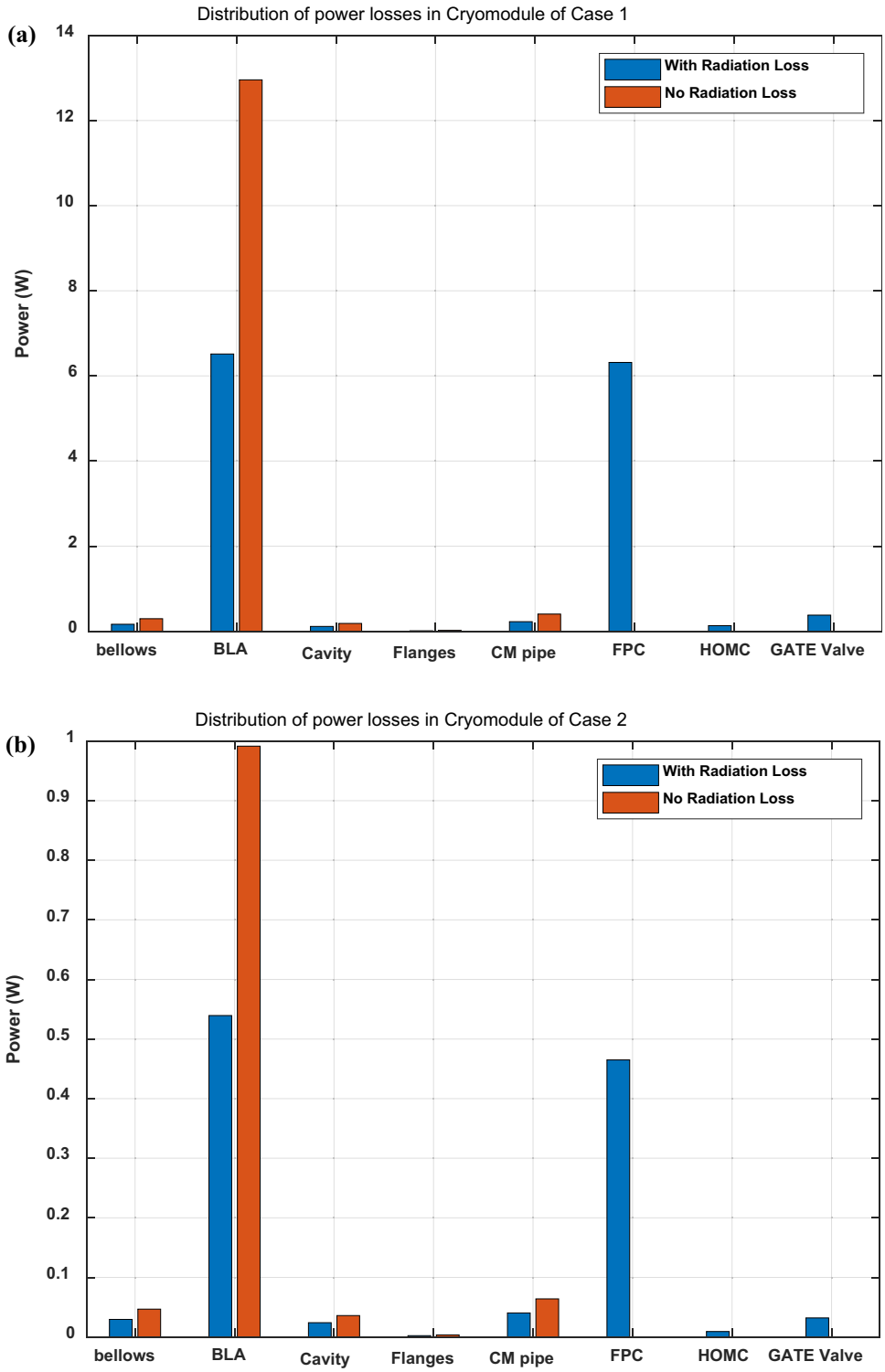

Fig. 12 (Color online) Distribution of total power losses in 1.3-GHz SHINE cryomodule L3 part for **a** Beam Case 1 and **b** Beam Case 2 with radiation loss and no radiation loss, respectively

power losses caused by the beam and deposited on each element of the linac were studied in this paper.

Power losses generated by the beam contribute to longitudinal HOMs excited by the irises of nine-cell cavities and the resistive wall wake of the beam pipe. A longitudinal HOM can be characterized as a trapped HOM (below the cutoff frequency) or untrapped HOM (above the cutoff frequency) according to the cutoff frequency of the beam pipe. Because it is below the cutoff frequency of the beam pipe, a trapped HOM can only remain in the cavity, causing power losses therein. An untrapped HOM causes power losses in every element of the SHINE 1.3-GHz Tesla-type

cryomodule because it can propagate through the cryomodule.

From the results regarding trapped HOMs, it is concluded that power losses in the two beam cases owing to resonance excitation of the longitudinal monopole HOM are very small. The median power loss, which corresponds to a probability of 0.5, is approximately 1 μW for trapped modes of the 1.3-GHz Tesla-type cavity in Case 1. Periodically, owing to random variations in its frequency, a single HOM in one cavity may come close to resonance. In this case, power losses in the 1.3-GHz Tesla-type cavity may increase to 100 mW, although the probability of such an event is extremely low at less than 1 mW. Comparing Case 1 and Case 2, we conclude that the lower the Q_b and f_{rep} of the bunch, the smaller the power losses.

From the results regarding untrapped HOMs, steady-state losses and transient losses generated by an untrapped HOM in L1, L2, and L3 were estimated. The heat load caused by resistive wall wakefields contributed as well. We found that most of the power is absorbed by the beam line absorber. This provides us some confidence in the effectiveness of the beamline HOM absorbers, suggesting that no more than a few percent of this power will present an added load to the 2-K cryogenics system.

Based on this study, these calculations will provide a reliable basis for the future construction of the SHINE linac.

Acknowledgements We are grateful to Prof. Vyacheslav Yakovlev of Fermilab and Prof. Igor Zagorodnov of DESY. They provided invaluable guidance and suggestions. We are also grateful to many of the staff members at the LINAC group of the FEL department SINAP for their support with ideas and discussions.

References

1. Z.Y. Zhu, Z.T. Zhao, D. Wang et al., SCLF: an 8-GeV CW SCRF linac-based X-ray FEL facility in Shanghai, in *Proceedings of the FEL2017, Santa Fe, NM, USA* (2017), p. 20. https://doi.org/10.18429/jacow-fel2017-mop055
2. C. Feng, H.X. Deng, Review of fully coherent free-electron laser. Nucl. Sci. Tech. **29**, 160 (2018). https://doi.org/10.1007/s41365-018-0490-1
3. Z.T. Zhao, C. Feng, K.Q. Zhang, Two-stage EEHG for coherent hard X-ray generation based on a superconducting linac. Nucl. Sci. Tech. **28**, 117 (2017). https://doi.org/10.1007/s41365-017-0258-z
4. Z. Wang, C. Feng, Q. Gu et al., Generation of double pulses at the Shanghai soft X-ray free electron laser facility. Nucl. Sci. Tech. **28**, 28 (2017). https://doi.org/10.1007/s41365-017-0188-9
5. K. Bane, T. Raubenheimer, A. Romanenko et al., Wakefields in the superconducting RF cavities of LCLS-II, in *Proceedings of LINAC2014, Geneva, Switzerland*, *THPP124*, pp. 1147–1150
6. Z. Wang, C. Feng, D.Z. Huang et al., Nonlinear energy chirp compensation with corrugated structures. Nucl. Sci. Tech. **29**, 175 (2018). https://doi.org/10.1007/s41365-018-0512-z
7. B. Aune, R. Bandelmann, D. Bloess et al., Superconducting TESLA cavities. Phys. Rev. Spec. Top. Accel. Beams **3**, 092001 (2000). https://doi.org/10.1103/PhysRevSTAB.3.092001
8. I. Zagorodnov, T. Weiland, The short-range transverse wake fields in TESLA accelerating structure, in *Proceedings of PAC03, Portland, Oregon, USA, RPPG034*, pp. 3249–3251
9. A. Saini, A. Lunin, N. Solyak et al., RF losses in 1.3 GHz cryomodule of the LCLS II superconducting CW linac, in *Proceedings of LINAC2016, East Lansing, MI, USA, THPRC014*, pp: 798-801
10. CST-Computer Simulation Technology, http://www.cst.com
11. H. Padamsee, J. Knobloch, T. Hays, *RF Superconductivity for Accelerators* (Wiley, New York, 1998)
12. A. Sukhanov, A. Vostrikov, T. Khabiboulline et al., Resonant Excitation of High Order Modes in Superconducting RF Cavities of LCLS II Linac. LCLS-II TN-15-06, March 2 (2015)
13. T. Khabiboulline, A. Sukhanov, N. Solyak et al., Resonance excitation of longitudinal high order modes in Project X Linac, in *Proceedings of IPAC2012, New Orleans, Louisiana, USA, WEPPC054,* pp. 2336–2338
14. A. Sukhanov, A. Lunin, V. Yakovlev et al., High order modes in Project-X linac. Nucl. Instrum. Methods Phys Res. A **734**, 9–22 (2014). https://doi.org/10.1016/j.nima.2013.06.113
15. N. Mildner, M. Dohlus, J. Sekutowicz et al., A beam line HOM absorber for the European XFEL linac, in *Proceedings of the 12th International Workshop on RF Superconductivity, Cornell University, Ithaca, New York, USA, THP55*, pp. 593–595
16. D. Kostin, J. Sekutowicz, W.D. Moeller et al., HOM coupler design adjustement for CW operation of the 1.3 GHZ 9-cell TESLA type SRF cavity, in *Proceedings of SRF2013, Paris, France, THP059*, pp. 1051–1054
17. G. Stupakov, K. Bane, P. Emma et al., Resistive wall wakefields of short bunches at cryogenic temperatures. Phys. Rev. Spec. Top. Accel. Beams **18**(3), 034402 (2015). https://doi.org/10.1103/PhysRevSTAB.18.034402
18. L. Palumbo, V. G. Vaccaro, M. Zobov, Wake fields and impedance, in *Advanced accelerator physics. Proceedings, 5th Course of the CERN Accelerator School, Rhodos, Greece, September 20–October 1*, 1993, Vol. 1, 2, pp. 331–390
19. K. Bane, Short-Range Dipole Wakefields in Accelerating Structures for the NLC, SLAC-PUB-9663, LCC-0116 (2003)
20. Code ECHO, http://www.desy.de/∼zagor
21. A. Novokhatski, M. Timm, T. Weiland, Single Bunch Energy Spread in the TESLA Cryomodule, DESY TESLA-99-16 (1999)
22. M. Song, C. Feng, D. Huang et al., Wakefields studies for the SXFEL user facility. Nucl. Sci. Tech. **28**, 90 (2017). https://doi.org/10.1007/s41365-017-0242-7
23. K. Bane, C. Nantista, C. Adolphsen et al., Distribution of heating from untrapped HOM radiation in the LCLS II cryomodules. Phys. Procedia **79**, 13–20 (2015). https://doi.org/10.1016/j.phpro.2015.11.057
24. A. Lunin, A. Saini, N. Solyak et al., Generation and Absorption of the Untrapped Wakefield Radiation in the 3.9 GHz LCLS-II Cryomodule, LCLS-II TN-16-06, July 11 (2016)